J. Min. Metall. Sect. B-Metall. 58 (2) (2022) 219 - 228

Journal of Mining and Metallurgy, Section B: Metallurgy

CHARACTERIZATION OF PRE-ALLOYED NiTi POWDERS PRODUCED BY ELECTRODE INDUCTION-MELTING INERT GAS ATOMIZATION FOR ADDITIVE MANUFACTURING

J.-W. Wang [a], D.-Y. He [a,b], X. Wu [a*], X.-Y. Guo [a], Z. Tan [a], Z. Zhou [a], W. Shao [a]

[a] Institute of Welding and Surface Engineering Technology, Faculty of Materials and Manufacturing, Beijing University of Technology, Beijing, China

[b] Beijing Engineering Research Center of Eco-materials and LCA, Beijing, China

(Received 19 October 2021; Accepted 06 May 2022)

Abstract

In this research, the characteristics of nickel-titanium (NiTi) powders produced by electrode induction melting inert gas atomization (EIGA) technique for additive manufacturing (AM) technology are investigated using various powder characterization technologies. The results show that the particle size distribution (PSD) of pre-alloyed NiTi powders prepared by EIGA has the range of 10 μm to 180 μm. The mean particle size distribution (D_{50}) of the powder is 75 μm. The oxygen increase of the powder is only 0.005% compared to the raw rod. According to the requirements of the characteristics of the metal powder material used for AM, the powders are sieved into three categories, P1 (15-63 μm), P2 (63-150 μm), and P3 (>150 μm), respectively. The flow rates of P1 and P2 are 19.3 and 17.5 s·(50 g)$^{-1}$, respectively. The surface, cross-sectional microstructure, phase structure, and martensitic transformation temperature of the pre-alloyed NiTi powders with different particle sizes are investigated. The results show that powders of different particle sizes are primarily spherical or nearly spherical. The grain size of powders reduces with the decreasing of particle size. Both the bar stock and the powders of P1, P2, and P3 mainly exhibit the B2 phase. Comparing the powders P1, P2, and P3, the transformation temperature reduces with the decrease of particle size. A high density (99.55%) pre-alloyed NiTi specimen is successfully produced by selective laser melting (SLM) technology using P1 powders. The results indicate that the pre-alloyed NiTi alloy powder is appropriate for AM, which also has a good reference value for researchers producing AM powders.

Keywords: *NiTi; Powder characteristics; EIGA; Selective laser melting; Martensitic transformation temperature*

1. Introduction

Nickel-titanium (NiTi) alloy is a prominent shape memory alloy (SMA) that is extensively applied in aerospace, automobiles, and medical implants, owing to its good biocompatibility, corrosion resistance, and interesting superelasticity (SE) and shape memory effect (SME) [1, 2]. However, the poor machinability of the alloy using conventional machining processes brings high costs and limits the development of nickel-based components [3, 4]. In the past decade, with the development of additive manufacturing technology, the preparation of NiTi parts circumvented many of the challenges faced by traditional processing methods. These processes are based on computer-designed three-dimensional data and required adding powder in successive layers and melted, in general, using a laser as the energy source [5]. For the preparation of high-quality NiTi components, the powder has requirements of low oxygen content, hydrogen content, high purity, high sphericity, and specific particle size characteristics [6]. Therefore, NiTi powder is the basis for the preparation of high-quality AM specimens. At present, pre-alloyed powder or a mixture of elemental powders of Ni and Ti is used as the raw powder for AM. It is noteworthy that pure nickel, pure titanium, and intermetallic phases were found in AM parts prepared using elemental blend powders [7]. Nowadays, pre-alloyed NiTi powder is mainly used as the raw material for AM process, due to the uniform distribution of each element in the powder. High-quality pre-alloyed powders are mainly prepared by Electrode Induction Melting Gas Atomization(EIGA) and Plasma Rotating Electrode Processing(PREP) methods, which integrate non-contact melting methods and outstanding vacuum conditions to prevent the hazards of crucible impurities and gaseous elements. Moreover, compared to the PREP method, the powders prepared by the EIGA process show a

* *Corresponding author: wuxu@bjut.edu.cn*

https://doi.org/10.2298/JMMB211019006W

high fine preparation rate and narrower average particle size distribution (D_{50}) [8, 9]. As a result, the EIGA technique has developed into an outstanding method of manufacturing high-quality characteristic pre-alloyed powders.

In the AM process, the printing process and the quality of parts are determined by the printing process parameters as well as pre-alloyed powder. For case in point, Li et al. [1] noticed that the Ti_2Ni phase in the SLMed specimen originated from the feedstock NiTi powder, and the powder with entrapped pores contributed to the residual porosity in the AM buildings. Haberland et al. [10] studied the phase transformation behavior between the additively manufactured NiTi parts with the feedstock NiTi powders of different compositions. They reported that the phase transformation temperature of NiTi parts was diminished with the content of Ni increasing. In TC4 titanium alloy, Qian et al. [11] also found that the defects and microstructure of the SLM specimens were correlated with the feedstock powder. The EIGA process involves a complex process from the melting of the bar, the disintegration of the droplets and the rapid cooling, which has a great impact on the properties of the powder. Also, the raw powders are sieved into different particle sizes to improve the utilization and accommodate the different additive manufacturing technologies. For instance, the powder particle sizes of 15 μm to 63 μm and 50 μm to 150 μm are used for Selective Laser Melting (SLM) and Laser Engineered Net Shaping (LENS), in the AM of NiTi alloys [12, 13]. However, the variation and differences in performance from bar to powder and sieving of powders with different particle size distributions for corresponding AM technology have not been studied in detail. Therefore, the characterization of NiTi powders is fundamental to fully appreciate the effect of the EIGA preparation procedure on the powders, as well as for the additive manufacturing of high-quality NiTi parts.

In this article, the variation of structure and properties of powders that were sieved into different particle size distributions were studied for the application in the different AM technology. Specifically, the particle size distribution (PSD), the particle shape, surface texture, micromorphology, martensite transformation of pre-alloyed NiTi powders, and the correlation between raw rod and powders was focused on in this paper. In addition, the structure as well as the property variation between the raw rod and the powders prepared by the EIGA was also investigated.

2. Experimental procedures

In the research, pre-alloyed NiTi bar was used as the raw material, and the composition was Ni (50 at.%)-Ti (50 at.%). The ingot was prepared by plasma arc cold hearth melting (PACHM). In order to properly feed into the EIGA equipment, the raw pre-alloyed NiTi was lathed into a bar stock of 50 mm in diameter and 500 mm in length (Figure 1a). Then, the bar stock was atomized by the EIGA technique of ALD Vacuum Technology GmbH (Germany). Especially, during the EIGA procedure, it was essential to maintain a high-quality vacuum and manage the pressure of atomization gas [14-16]. To ensure a high vacuum level during the atomization procedure, the internal air of the EIGA device was evacuated until the air pressure was dropped to 3.0×10^{-3} Pa. The exceedingly low-level of vacuum state guaranteed the low increment of oxygen content in the preparation of alloy powders. Afterward, high-purity argon gas was purged into the melting chamber and the atomization chamber to maintain the pressure at 1.2×10^{5} Pa and 1.0×10^{5} Pa, respectively, with a suitable pressure difference. Lastly, in the melt chamber, the NiTi alloy bar stock was fused by the induction coil heat source. In the atomization chamber, the droplets were quickly broken by high-pressure argon gas and cooled under argon atmosphere, and finally the NiTi powder was prepared. Figure 1b, c clearly showed the melting process of pre-alloyed NiTi bar stock in the melt chamber, and the remainder after the EIGA process. In this study, the main EIGA process parameter of melting power, atomization pressure, and feed rate were 30kW, 3MPa and 55mm·min^{-1}, respectively.

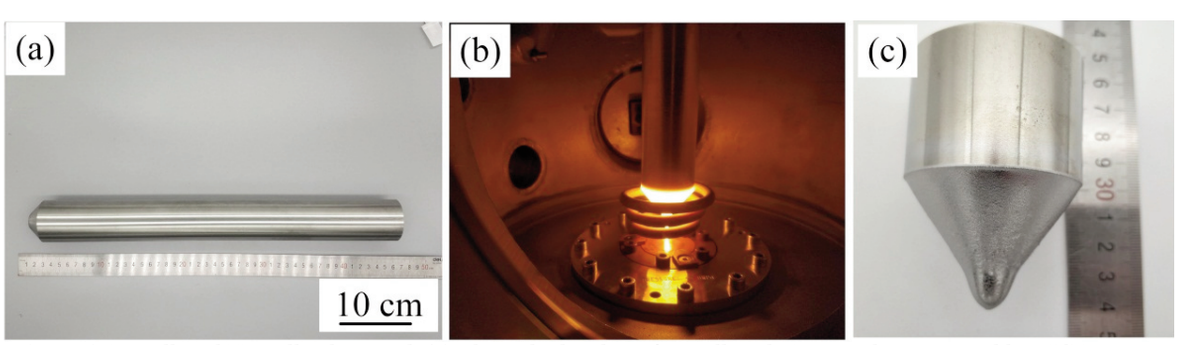

Figure 1. *Pre-alloyed NiTi alloy bar stock (a); the melt chamber of pre-alloyed NiTi powders prepared by EIGA process (b), the remainder of pre-alloyed NiTi bar stock after EIGA process (c)*

The equiatomic pre-alloyed NiTi powders were produced by the EIGA process with argon gas. The large particle size range of the original powders prepared by EIGA was not suitable for immediately using in AM process [17]. Therefore, the pre-alloyed powders prepared by the EIGA process were sieved into three categories, according to the powder particle size, ≤63 μm (P1), 63-150 μm (P2), and ≥150 μm (P3), respectively. For this research, the powder flowability was me asured according to the ASTM B213 standard by a Hall flowmeter. Apparent density and tapped density were measured according to the ASTM B212 and ASTM B527 standards. The Waddell sphericity of the powders in this study were measured by SEM images analysis. The corresponding average values were obtained from five determinations and were shown in Table 1. The phase compositions of ingot, P1, P2, and P3 were measured by X-ray diffraction (XRD, Bruker D8 Advance Phaser), Cu Kα radiation target, at room temperature. In order to investigate the internal microstructure of the powder, cross-sectional metallographic specimens were obtained by mounting the powder particles in epoxy resin, machine-polished by SiC papers, and etched by Kroll's reagent. The surface and cross-sectional microstructural characterization of the powders were performed by Scanning electron microscopy (SEM, FEI QUANTA FEG 650) equipped with energy-dispersive X-ray spectrometry (EDX). The main elements were determined by gravimetric analysis. The content of oxygen and nitrogen elements was measured by inert gas fusion analysis instruments (Bruker G8 Galileo). The transition temperatures (TTs) were measured by NETZSCH DSC 214, and the temperature range was -100 ºC -150 ºC with a heating/cooling rate of 10 ºC /min, in the argon atmosphere. The SLMed parts were fabricated by EOS M100 Systems with a 200 W Ytterbium fiber laser.

Table 1. *Wadell sphericity, Hall flow rate, apparent density, and tapped density of P1, P2 and P3*

Powder	Wadell sphericity (%)	Flowability ($s \cdot (50g)^{-1}$)	Apparent density (g/cm^3)	Tapped density (g/cm^3)
P1	95.7 ± 0.4	19.3 ± 0.2	3.40 ± 0.03	4.24 ± 0.04
P2	93.5 ± 0.6	17.5 ± 0.1	3.16 ± 0.02	4.11 ± 0.04
P3	58.7 ± 0.9	15.8 ± 0.1	3.07 ±0.02	4.08 ± 0.03

3. Results and discussion

3.1. Physical properties of pre-alloyed NiTi powders

Figure 2 indicates the morphology and particle size distribution of raw pre-alloyed NiTi powders. The shape of raw powders is spherical or nearly spherical, few satellites and metal fragments can be observed, as shown in Figure 2a. The particle size distribution of the original powders is one of the most fundamental results, as the specific distribution determines the yielding rate of pre-alloyed NiTi powders prepared by EIGA for different particle size distribution ranges.

Figure 2b displays the particle size distribution of the original NiTi powders obtained by the EIGA process. It is observed that the particle size range of the original NiTi powder is 10 to 180 μm. The mean particle size distribution (D_{50}) of the original NiTi powders is 75 μm, and the number of the powder size from 20 to 150 μm occupies about 90%. In addition, powders with a particle size of less than 150 μm can be used in additive manufacturing technology. Nanoval process was another gas atomization technique for the preparation of pre-alloyed NiTi powders, which had the D_{50} of powders about 10 μm and a high percentage of powders less than 45 μm [18]. The presence of a large amount of fine powder (<10 μm) causes the fluidity of the powder to fails to satisfy the requirements of AM technology. In contrast, the mean particle size of pre-alloy NiTi powders prepared by the EIGA process is larger than

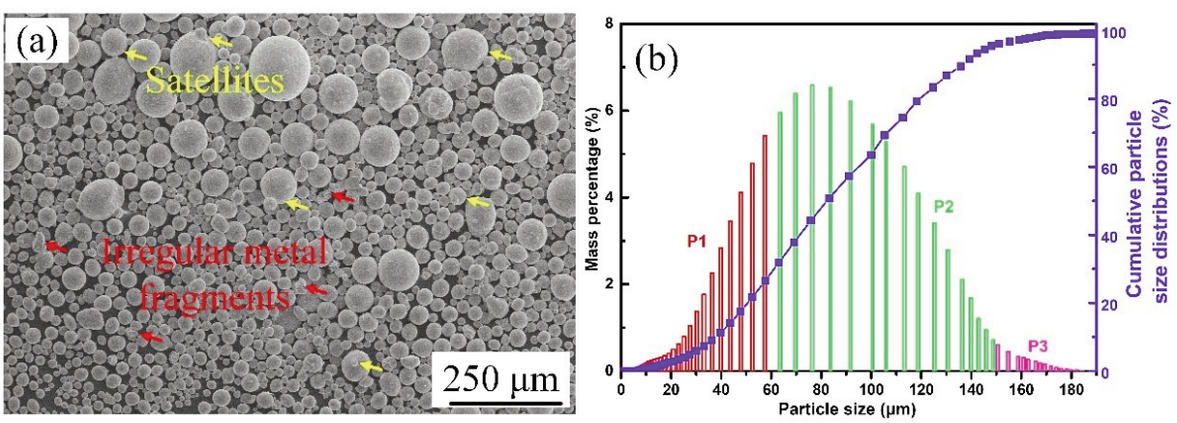

Figure 2. *(a) Morphology and (b) particle size distribution of raw NiTi powders prepared by EIGA process*

that produced by Nanoval process, which is more suitable for additive manufacturing.

In AM technology, the flowability of NiTi powder is very significant, and the poor flowability of the powder increases the possibility of problems in the procedure of the deposition process. The flowability of P1, P2, and P3 is 19.3, 17.5, and 15.8 $s \cdot (50g)^{-1}$, respectively, satisfying the requirement of AM technology (Table 1). It is superior to the commonly available Ti-6Al-4V powder used for EBM [19] and IN718 powder used for SLM [12], which means that pre-alloyed NiTi powders are a well-suited material for AM process. The flowability increases with the increase of powder size. Because the smaller particle size of the powders, the higher the adhesion force between the powders, the powders are easy to adhere together, resulting in the decreasing of flowability. The density of the powder affects the density and defects of the parts prepared by AM. In this paper, the apparent density and tapped density of pre-alloyed NiTi powders were measured. Table 1 illustrates the flowability, apparent density, and tapped density of pre-alloyed NiTi powders prepared by EIGA for P1, P2, and P3, respectively. The apparent density and tapped density of P1, P2 are 3.40 $g \cdot cm^{-3}$, 4.24 $g \cdot cm^{-3}$ and 3.16 $g \cdot cm^{-3}$, 4.11 $g \cdot cm^{-3}$ (Table 1). The density of the corresponding bar stock is 6.15 $g \cdot cm^{-3}$. The apparent density ratio of P1, P2 is more than 50%, which fulfills the requirements of AM technology for apparent density. The fact is that apparent density and tapped density increase with the increase of powder particle size. The fine spherical particles have a higher apparent density and tapped density than the coarse ones.

3.2. Morphology of pre-alloyed NiTi powders

The morphology of the powder is directly connected to the flowability and density of the powder. The SEM images of P1, P2 (used for AM), and P3 are displayed in Figure 3. As shown in Figure 3, the majority of powders (P1, P2) are spherical or near-spherical, with a limited number of oval particles and a comparatively low concentration of satellites.

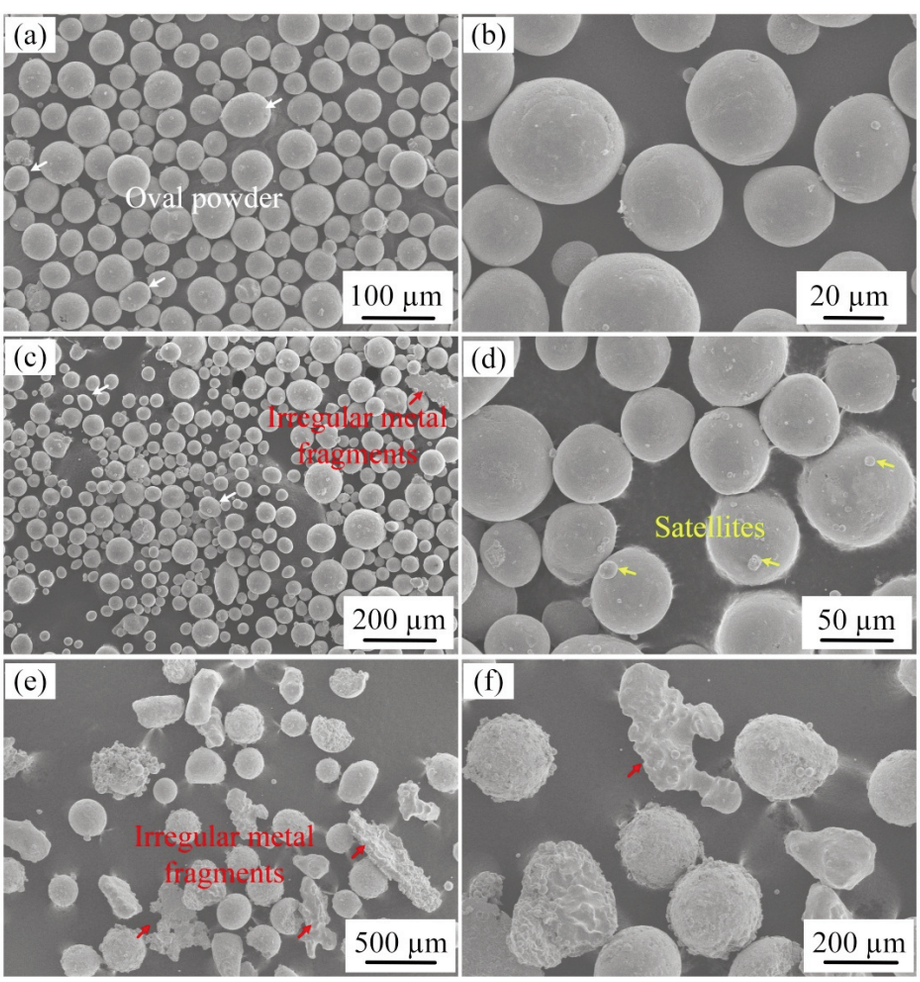

Figure 3. *SEM images of pre-alloyed NiTi powders with different sizes: (a) and (b) P1, (c) and (d) P2, (e) and (f) P3*

The Wadell sphericity of P1, P2 and P3 are 95.7%, 93.5%, and 58.7% respectively (Table 1). This ensures that P1 and P2 have a good flowability to fulfill the requirements of AM technology. Comparing the morphology of P1, P2, and P3, the oval particles and satellites are less seldom found in P1, the number increases in P2. However, a large number of irregular metal fragments appear in P3 (Figure 3). Compared to the infrequent appearance in the P1 (Figure 3a), the amount of oval and satellites increases in P2 (Figure 3c, d). The main reason for the formation of irregular powder is that the larger powder particles exhibit less surface tension, resulting in a greater solidification rate of the droplets than the shrinkage rate. With the increase of powder particle size, the powder collision between each other will also make the powder shape irregular. Satellite particles are generated by the collision of solidified droplets caused by turbulence in the atomization chamber. With the increase of powder particle size, the chance of adhering to fine powder on its surface also increases, which leads to the increasing number of the satellites. These can influence the flowability of pre-alloyed NiTi powders. It can be found that the flowability of pre-alloyed NiTi powders (P1, P2) is less than 20 $s \cdot (50g)^{-1}$, which satisfies the requirements of AM technology (Table 1). A large number of irregular metal fragments appear in P3, probably due to the collision of the solidified particles with the wall under high-pressure gas. The SEM images of the pre-alloyed NiTi powders (P1, P2) cross-sectional morphology are shown in Figure 4a, b. The pre-alloyed NiTi powder is very dense, without the appearance of holes in it, which provides a guarantee for the preparation of dense AM parts (Figure 4a, b).

3.3. Element composition of pre-alloyed NiTi powders

Table 2 shows the analysis of the chemical composition, which indicates that the Ni and Ti elements are close to equimolar composition in pre-alloyed NiTi bar stock and powders. From the bar stock to the raw pre-alloyed NiTi powders prepared by the EIGA process, the elemental content of the powder has only a slight difference, with the oxygen content of 0.064%. Compared with the bar, the increment of raw powders is only 0.005%, which is attributed to the use of Ar as the shield gas and the high vacuum level in the EIGA process. The element content distribution of Ni and Ti is observed in the EDS mapping (Figure 4c). As indicated from the EDS image inside of the powder (Figure 4c), the Ni and Ti elemental distribution is uniform. This is attributed to the uniform distribution of the components of the original bar stock and the extremely rapid cooling rate (104-107K/s) during the EIGA process, resulting in insufficient time for the segregation of elements in the alloy droplets before solidification [20].

Table 2. *Chemical composition of pre-alloy NiTi bar stock and powders*

Elements	Ni (wt./%)	O (wt./%)	H (wt./%)	N (wt./%)	Ti (wt./%)
Bar stock	55.67	0.059	<0.0010	<0.0030	Bal.
Powder	55.54	0.064	<0.0010	<0.0030	Bal.

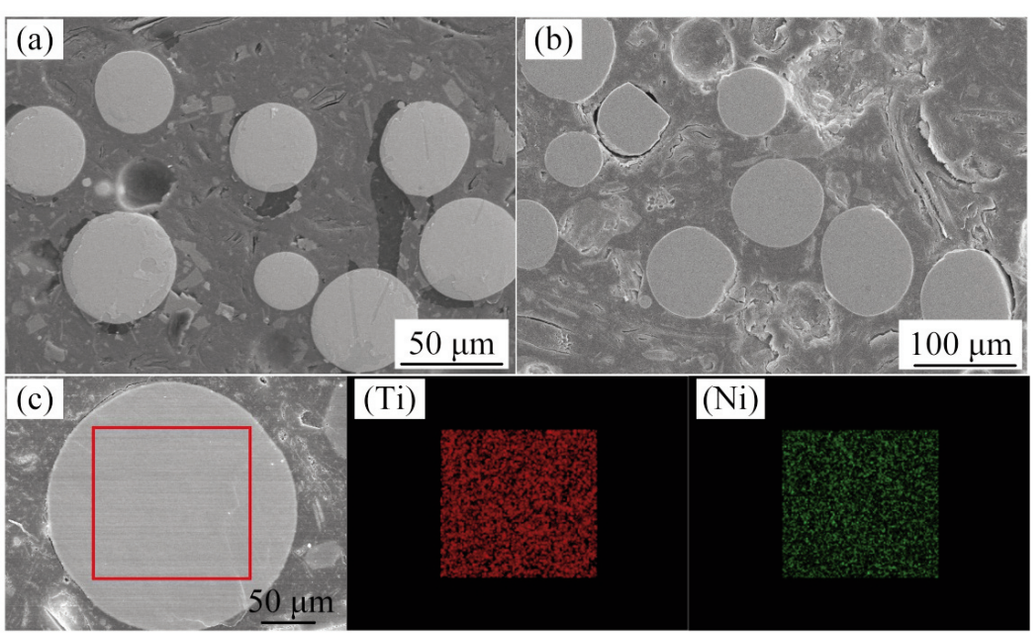

Figure 4. *Cross sectional SEM images of pre-alloyed NiTi powders: (a) for P1, (b) for P2, and EDS analysis (c)*

3.4. Microstructure and phase constituents of pre-alloyed NiTi powders

The microstructures of the cross-sectional powders (P1, P2, and P3) after etching are shown in Figure 5. The majority of the inner grain microstructures of powders with different grain sizes are equiaxed, with only a difference in grain size (Figure 5). For instance, the average grain sizes of P1, P2, and P3 are about 3, 5, and 10 μm, respectively (Figure 5b, d, f). In addition, comparing the variation of the average grain size for P1, P2, and P3, the grain size gradually enlarges with the increase of powder size (Figure 5). Solidification rate and temperature gradient are the main factors affecting the internal grain morphology of the powder [21]. Compared to a temperature gradient, a high solidification rate is the main reason for the formation of equiaxial grain structure inside the powder during solidification. This condition is consistent with studies where increasing surface cooling rate or super cooling layers to obtain equiaxial morphology, and both in that higher cooling rates will be more likely to lead to equiaxial structures, regardless of temperature gradients. The higher cooling rates will be more likely to lead to equiaxed structures without considering the temperature gradient [22, 23]. In this study, the pre-alloyed NiTi powders (P1, P2 and P3) have equiaxial grains, with a high cooling rate during the EIGA process. The fine powder has a higher solidification rate, which makes the grain size finer.

The phase composition patterns of bar stock, P1, P2, and P3, tested at room temperature by XRD, are shown in Figure 6. The bar stock and the pre-alloyed NiTi powders with different particle sizes exhibit primarily in the B2 austenite phase of the Miller indices (110), (200), and (211), with a few amounts of B19' martensitic phase, at room temperature. In comparison, it can be found that the diffraction peak intensity is almost the same between P3 and bar stock, with the same Miller indices (020) of B19'. The B19' Miller indices of P1, P2 is (111). As the particle size of the powder decreases (from P3 to P1), the corresponding intensity of the diffraction peak is increasing (Figure 6). It is possible that the finer powders have the faster cooling rate. The grains are easy to grow in the corresponding texture direction, resulting in the increasing of diffraction peak intensity.

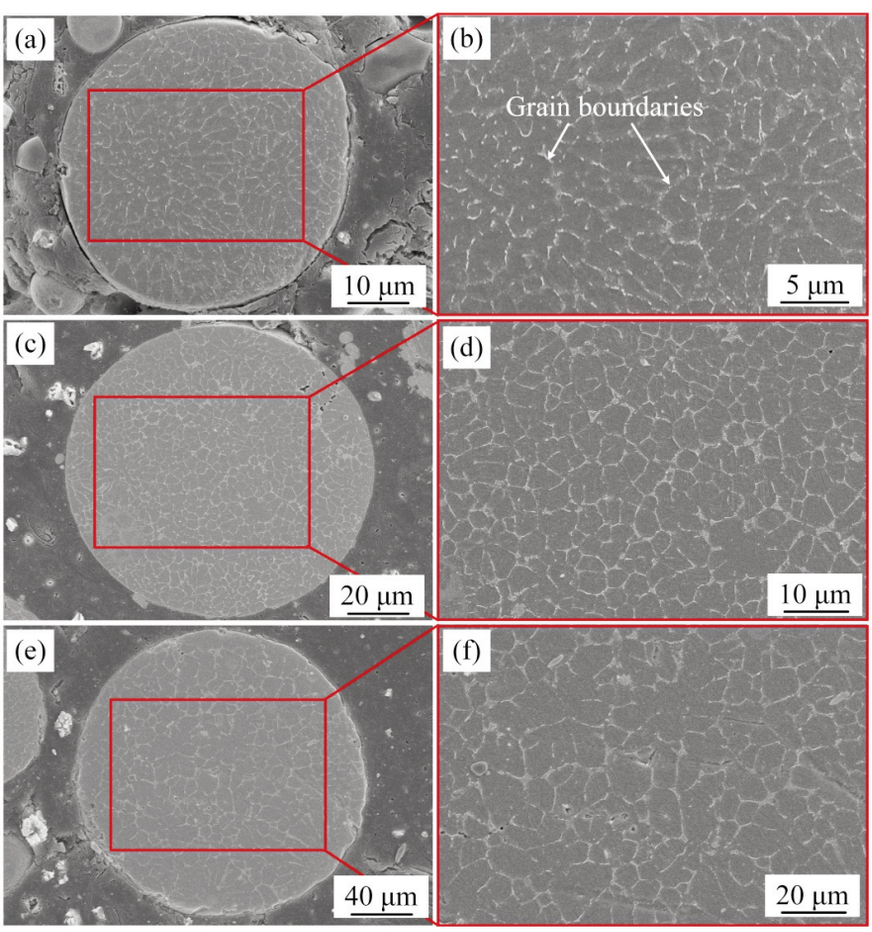

Figure 5. *Cross sectional microstructures of pre-alloyed NiTi powders: (a, b) P1, (c, d) P2, (e, f) P3*

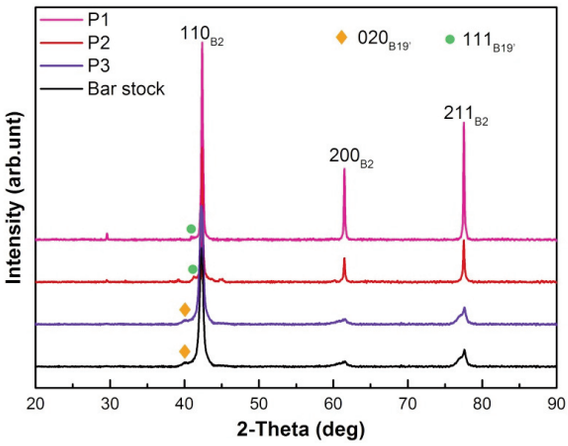

Figure 6. X-ray diffraction patterns of the bar stock, and pre-alloyed NiTi powders of P1, P2, P3

3.5. Transformation temperature of bar stock and pre-alloy NiTi powders

Figure 7 illustrates the DSC curves of the initial bar stock, and the powders of P1, P2, and P3. The values of transformation temperatures (TTs) obtained from Figure 7, specifically including the martensite start (M_s) temperature, martensite finish (M_f) temperature, austenite start (A_s) temperature, and austenite finish (A_f) temperature, are shown in Table 3. Three significant phenomena are obtained from Figure 7 and Table 3. In the first place, the TTs of P1, P2, and P3 are increased in comparison to the initial bar stock. Secondly, comparing the TTs of the powders with different particle sizes, the TTs increase with the increasing particle size of P1, P2, and P3. Finally, during the cooling process, only one peak appears in the phase transition process of the bar stock, while the powder of P1, P2, and P3 shows two or even more peaks (Figure 7), due to the inhomogeneity of the powder. The evaporation of elements is the main

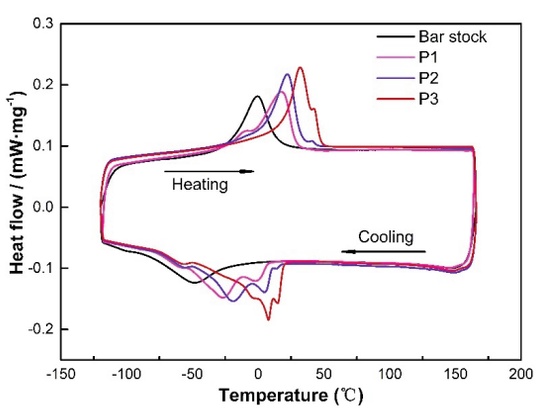

Figure 7. DSC curves of bar stock and pre-alloyed NiTi powders (P1, P2, P3) upon cooling and heating

Table 3. Transformation temperatures of bar stock and pre-alloyed NiTi powders (P1, P2, P3)

Specimen	M_s (ºC)	M_f (ºC)	A_s (ºC)	A_f (ºC)
Bar stock	-23	-82	-22	14
P1	7	-77	-24	29
P2	17	-75	3	45
P3	19	-74	19	48

reason for the increasing transformation temperature of the powders, compared with the bar stock. The fact is that the high temperature causes the evaporation of elements during the EIGA process. Compared to the evaporation temperature of titanium and nickel, the evaporation temperature of nickel is lower. Therefore the composition of the powder shifts to a lower nickel content, which is also evidenced by the variation of nickel content in Table 2. For NiTi alloys with near isoatomic ratios, the transition temperature decreases with the increase of nickel [24]. The transition temperature increases with the increase of powder size of P1, P2, and P3, due to the increase of grain size inside the powder (Figure 5). As the grain size inside the powder increases, the yield strength of the parent phase (B2) decreases. This results in less resistance to be overcome in the shear transformation of the parent phase. Ultimately, this leads to a reduction in the driving force required for the phase transition and an increase in the corresponding transition temperature. Waitz et al [25] spotted that the martensitic phase transformation is depressed with the decreasing of grain size in NiTi alloy. This conclusion is also confirmed in the case of NiTi powder.

In order to investigate the thermal cycling stability of the pre-alloy NiTi powders prepared by EIGA, P1 is selected for characterization in this study. It fulfills the powder particle size requirements for SLM of the one of most popular technology in AM. Figure 8 shows the DSC curves of powder (P1) for 10 cycles.

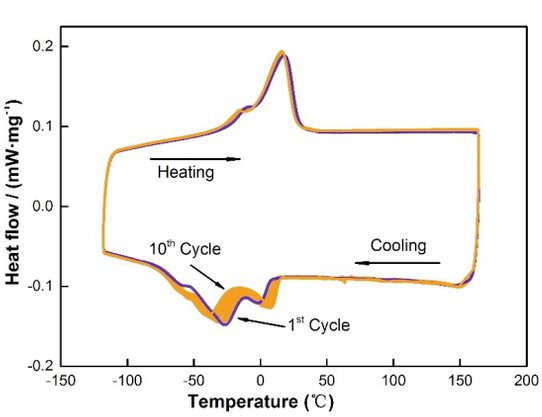

Figure 8. Thermal cycling behavior of the pre-alloy NiTi powders (P1)

The transformation temperatures stabilized with thermal cycling. The A_f and M_s temperatures of the powder changed from 27 ºC and 10 ºC in the first cycle to 26 ºC and 14 ºC in the 10th cycle.

3.6. Process development for SLM pre-alloyed NiTi alloy

In order to verify the printability of pre-alloyed NiTi powders prepared by EIGA, NiTi specimens were printed using the P1 by SLM, one of the most popular technologies in AM. Based on the requirement of the high density of SLM parts, specimens with a density of over 99% (measured by image method) were obtained by continuous optimization of the SLM process. Figure 9 displays the image of as-built SLM pre-alloyed NiTi parts and three-dimensional morphology built by top and side view of the densest specimen. The top surface view of the cube-shaped specimen and side view (after being polished) are shown in Figure 9b. With the corresponding energy input and reasonable construction temperature, the specimen with high-density (99.55%) and fully melted of a relatively uniform top surface can be obtained (Figure 9b).

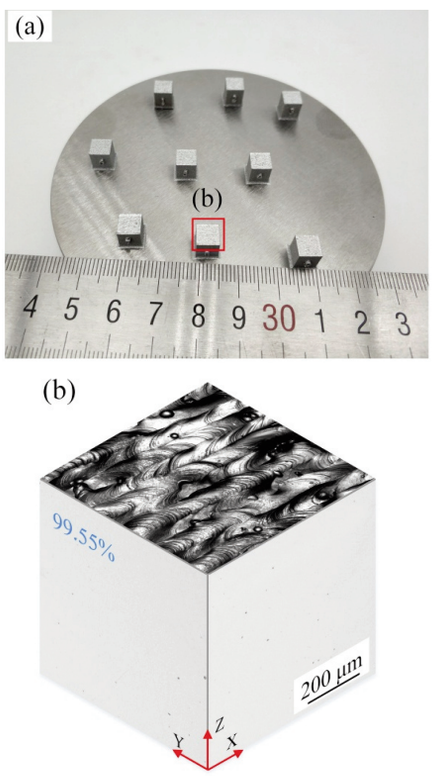

Figure 9. *(a) Image of pre-alloyed NiTi cuboid specimens by SLM. (b) Three dimensional morphology built by top and side view (after polished)*

4. Conclusions

The NiTi alloy powder was successfully prepared by the EIGA technology at a melting power of 30 kW, atomization pressure of 3 MPa, and feeding rate 55 $mm \cdot min^{-1}$. The particle size distribution (PSD) indicated that the range of NiTi alloy powders prepared by the EIGA is from 10 μm to 180 μm. The mean particle size distribution (D_{50}) of the powder is 75 μm.

The powder has a uniform distribution of chemical elements with an oxygen content of 0.060%, which is only 0.005% higher than the raw material. The XRD results reveal that the bar stock and the NiTi powders with various particle sizes mainly contain the austenite B2 phase.

Compared with the initial bar stock, the transformation temperatures (TTs) of the powder were increased. Comparing the TTs of powders with different particle sizes, the TTs increase with the increasing particle size of P1, P2, and P3. For the pre-alloy NiTi powders of P1, the transformation temperature is stable during the thermal cycle process.

Acknowledgments

This work is supported by financial support from the National Key R&D Program of China (No. 2018YFC1901701), the National Natural Science Foundation of China (Grant No. 51901004), and the Project of Science and Technology Commission of Chaoyang District, Beijing (No. CYXC1801).

Author's Contributions

Junwei Wang: Methodology, Writing-original draft, Investigation. Dingyong He: Resources, Funding acquisition, Supervision. Xu Wu: Conceptualization, Formal analysis, Writing-review & editing. Xingye Guo: Project administration. Zhen Tan: Software. Zheng Zhou: Data curation. Wei Shao: Visualization.

Data availability Statement

All data generated or analyzed during this study are included in this published article.

Declarations of interest

The authors declare that they have no conflict of interest.

References

[1] S. Li, H. Hassanin, M.M. Attallah, N.J. Adkins, K. Essa, The development of TiNi-based negative Poisson's ratio structure using selective laser melting, Acta Materialia, 105 (2016) 75-83. https://doi.org/10.1016/j.actamat.2015.12.017

[2] M.T. Andani, W. Anderson, M. Elahinia, Design, modeling and experimental evaluation of a minimally invasive cage for spinal fusion surgery utilizing superelastic Nitinol hinges, Journal of Intelligent Material Systems and Structures, 26 (6) (2015) 631-638. https://doi.org/10.1177/1045389X14541499

[3] M.H. Elahinia, M. Hashemi, M. Tabesh, S.B. Bhaduri, Manufacturing and processing of NiTi implants: A review. Progress in Materials Science, 57 (5) (2012) 911-946. https://doi.org/10.1016/j.pmatsci.2011.11.001

[4] J.M. Jani, M. Leary, A. Subic, M.A. Gibson, A review of shape memory alloy research, applications and opportunities, Materials & Design, 56 (2014) 1078-1113. https://doi.org/10.1016/j.matdes.2013.11.084

[5] M.T. Andani, N.-S. Moghaddam, C. Haberland, D. Dean, M.J. Miller, M. Elahinia, Metals for bone implants. Part 1. Powder metallurgy and implant rendering, Acta Biomaterialia, 10 (10) (2014) 4058-4070. https://doi.org/10.1016/j.actbio.2014.06.025

[6] H. Attar, K.G. Prashanth, L.C. Zhang, M. Calin, I.V. Okulov, S. Scudino, J. Eckert, Effect of powder particle shape on the properties of in situ Ti-TiB composite materials produced by selective laser melting, Journal of Materials Science & Technology, 31(10) (2015) 1001-1005. https://doi.org/10.1016/j.jmst.2015.08.007

[7] I. Shishkovsky, I. Yadroitsev, I. Smurov, Direct selective laser melting of nitinol powder, Physics Procedia, 39 (2012) 447-454. https://doi.org/10.1016/j.phpro.2012.10.060

[8] M.N. Ahsan, A.J. Pinkerton, R.J. Moat, J. Shackleton, A comparative study of laser direct metal deposition characteristics using gas and plasma-atomized Ti–6Al–4V powders, Materials Science and Engineering: A, 528 (25-26) (2011) 7648-7657. https://doi.org/10.1016/j.msea.2011.06.074

[9] Y. Huang, Y. Wang, H. Fan, J.A. Shen, A TiAl based alloy with excellent mechanical performance prepared by gas atomization and spark plasma sintering, Intermetallics, 31 (2012) 202-207. https://doi.org/10.1016/j.intermet.2012.07.006

[10] A.N. Alagha, S. Hussain, W. Zaki, Additive manufacturing of shape memory alloys: A review with emphasis on powder bed systems, Materials & Design, 204 (2021) 109654. https://doi.org/10.1016/j.matdes.2021.109654

[11] M. Qian, W. Xu, M. Brandt, H.P. Tang, Additive manufacturing and postprocessing of Ti-6Al-4V for superior mechanical properties, Mrs Bulletin, 41 (10) (2016) 775-784. https://doi.org/10.1557/mrs.2016.215

[12] Q.B. Nguyen, M.L.S. Nai, Z. Zhu, C.N. Sun, J. Wei, W. Zhou, Characteristics of inconel powders for powder-bed additive manufacturing, Engineering, 3 (5) (2017) 695-700. https://doi.org/10.1016/J.ENG.2017.05.012

[13] J.J. Marattukalam, A.K. Singh, S. Datta, M. Das, V.K. Balla, S. Bontha, S.K. Kalpathy, Microstructure and corrosion behavior of laser processed NiTi alloy, Materials Science and Engineering: C, 57 (2015) 309-313. https://doi.org/10.1016/j.msec.2015.07.067

[14] R. Todorović, M. Vujisić, D. Kovačević, K. Stanković, P. Osmokrović, Boundary area between gas and vacuum breakdown mechanism, Vacuum, 86 (12) (2012) 1800-1809. https://doi.org/10.1016/j.vacuum.2012.04.031

[15] Y. Sun, Y. Ren, New preparation method of porous copper powder through vacuum dealloying, Vacuum, 122 (2015) 215-217. https://doi.org/10.1016/j.vacuum.2015.09.031

[16] L. Zhang, J. Shao, X. Chen, CFD simulation of nozzle characteristics in a gas aggregation cluster source, Vacuum, 129 (2016) 105-110. https://doi.org/10.1016/j.vacuum.2016.04.020

[17] I.E. Anderson, E.M. White, R. Dehoff, Feedstock powder processing research needs for additive manufacturing development, Current Opinion in Solid State and Materials Science, 22 (1) (2018) 8-15. https://doi.org/10.1016/j.cossms.2018.01.002

[18] M. Bram M. Bitzer, H.P. Buchkremer, D. Stöver, Reproducibility study of NiTi parts made by metal injection molding, Journal of Materials Engineering and Performance, 21(12) (2012) 2701–2712. https://doi.org/10.1007/s11665-012-0264-6

[19] H.P. Tang, M. Qian, N. Liu, X. Zhang, G.Y. Yang, J. Wang, Effect of powder reuse times on additive manufacturing of Ti-6Al-4V by selective electron beam melting, JOM , 67 (3) (2015) 555-563. https://doi.org/10.1007/s11837-015-1300-4

[20] M. Zheng, S. Zhang, Q. Hu, H. He, Y. Sheng, X. Zhao, Microstructural characterisation of CuAgZr powder particles produced by argon gas atomisation, Powder Metallurgy, 61(3) (2018) 231-240. https://doi.org/10.1080/00325899.2018.1470288

[21] W. Kurz, B. Giovanola, R. Trivedi, Theory of microstructural development during rapid solidification, Acta Metallurgica, 34 (5) (1986) 823-830. https://doi.org/10.1016/0001-6160(86)90056-8

[22] F. Yan, W. Xiong, E.J. Faierson, Grain structure control of additively manufactured metallic materials, Materials, 10 (11) (2017) 1260. https://doi.org/10.3390/ma10111260

[23] Y. Zhang, L. Wu, X. Guo, S. Kane, Y. Deng, Y.G. Jung, J.H. Lee, J. Zhang, Additive manufacturing of metallic materials: a review, Journal of Materials Engineering and Performance, 27 (1) (2018) 1-13. https://doi.org/10.1007/s11665-017-2747-y

[24] S. Das, Physical aspects of process control in selective laser sintering of metals, Advanced Engineering Materials, 5 (10) (2003) 701-711.

[25] T. Waitz, The self-accommodated morphology of martensite in nanocrystalline NiTi shape memory alloys, Acta Materialia, 53 (8) (2005) 2273-2283. https://doi.org/10.1016/j.actamat.2005.01.033

KARAKTERIZACIJA PRETHODNO LEGIRANIH NiTi PRAHOVA NAMENJENIH PROIZVODNJI ADITIVA DOBIJENIH INDUKCIONIM TOPLJENJEM ELEKTRODA GASNOM ATOMIZACIJOM INERTNOG GASA

J.-W. Wang [a], D.-Y. He [a,b], X. Wu [a*], X.-Y. Guo [a], Z. Tan [a], Z. Zhou [a], W. Shao [a]

[a] Institut za zavarivanje i tehnologiju površinskog inženjerstva , Fakultet za materijale i proizvodnju, Tehnološki univerzitet u Pekingu, Peking, Kina
[b] Inženjerski istraživački centar za eko materijale i LCA u Pekingu, Peking, Kina

Apstrakt

U ovom istraživanju karakteristike nikl-titanijum (NiTi) prahova dobijenih tehnikom indukcionog topljenja elektroda gasnom atomizacijom inertnog gasa (EIGA), a za tehnologiju proizvodnje aditiva (AM), ispitivane su pomoću različitih tehnologija karakterizacije prahova. Rezultati pokazuju da je raspodela veličine čestica (PSD) prethodno legiranih NiTi prahova pripremljenih pomoću EIGA bila u opsegu od 10 μm do180 μm. Srednja distribucija veličine čestica je 75 μm. U poređenju sa sirovom šipkom, povećanje kiseonika u prahu je samo 0,005%. U skladu sa zahtevima karakterizacije materijala metalnog praha koji se koriste za AM, prahovi se prosejavaju u tri kategorije, P1 (15-63 μm), P2 (63-150 μm), i P3 (>150 μm), pojedinačno. Brzine protoka P1 i P2 je 19.3 i 17.5 $s \cdot (50\ g)^{-1}$, pojedinačno. Proučavani su površina, mikrostruktura poprečnog preseka, fazna struktura i temperatura martenzitne transformacije prethodno legiranih NiTi prahova različitih veličina čestica. Rezultati pokazuju da su prahovi različitih veličina čestica primarno sferni ili skoro sferni. Veličina zrna prahova smanjuje se sa smanjenjem čestica. I sirova šipka i prahovi P1, P2, i P3 pretežno pokazuju B2 fazu. Kada se prahovi uporede, temperatura transformacije se smanjuje sa smanjenjem veličine čestica. Velika gustina (99.55%) prethodno legiranog NiTi uzorka se uspešno postiže tehnologijom selektivnog laserskog topljenja (SLM) P1 prahova. Rezultati pokazuju da je prethodno legirani NiTi prah legure odgovarajući za AM, što je takođe dobra referentna vrednost za istraživače koji se bave proizvodnjom AM prahova.

Ključne reči: *NiTi; Karakteristike praha; EIGA; Selektivno lasersko topljenje; Temperatura martenzitne transformacije*